Transient and steady-state readout of nanowire gas sensors in the presence of low-frequency noise

Author(s):
Satterthwaite, Peter F.; Eberle, Sebastian; Nedelcu, Stefan; Roman, Cosmin; Hierold, Christofer

Publication date:
2019-10-15

Permanent link:
https://doi.org/10.3929/ethz-b-000351746

Originally published in:
Sensors and Actuators B: Chemical 297, https://doi.org/10.1016/j.snb.2019.126674

Sensors & Actuators: B. Chemical 297 (2019) 126674

Contents lists available at ScienceDirect

Sensors and Actuators B: Chemical

journal homepage: www.elsevier.com/locate/snb

Transient and steady-state readout of nanowire gas sensors in the presence of low-frequency noise

Peter F. Satterthwaite[a,b,*], Sebastian Eberle[b], Stefan Nedelcu[b], Cosmin Roman[b], Christofer Hierold[b]

[a] Electrical Engineering Department, Stanford University, Stanford, CA 94305, USA
[b] Micro and Nanosystems, ETH Zürich, CH-8092 Zürich, Switzerland

ARTICLE INFO

Keywords:
Nanowire sensors
Carbon nanotubes
Transient sensing
Gas sensing
1/f noise
Signal-to-noise ratio

ABSTRACT

Nanowire sensors show great promise in a variety of sensing applications due to their potential for high sensitivities. Practical nanowire sensor systems, however, are often limited by low-frequency, $1/f$ noise. This work presents theoretical and experimental results comparing the performance metrics of sensing schemes using transient and steady-state parameters in the presence of $1/f$ noise. Criteria are derived for when the considered transient or steady-state sensing schemes will have a better signal-to-noise ratio (SNR). The theoretical results for the SNR of these sensing schemes are applied to experimental data from carbon nanotube NO_2 sensors. These data and theoretical results demonstrate that due to the Langmuir binding behavior of the sensor-analyte system, sensing using the considered transient parameters increases linearity and decreases response time relative to steady-state sensing. Noise analysis further shows that with current devices, transient sensing has a lower SNR relative to steady-state sensing, however this may change if functionalization is considered. The use of transient parameters also has the potential to reduce sensor drift due to $1/f$ noise, improving system stability. In addition to providing useful considerations towards the design of carbon nanotube gas sensors, these results are relevant towards understanding the SNR of other chemical and biological sensors limited by $1/f$ noise.

1. Introduction

Sensors based on nanowire devices have been demonstrated in a variety of chemical and biological sensing applications [1–5]. The nanoscale nature of these devices is key to their high sensitivity, due to the large surface to volume ratio in nanowire devices. Yet, these same nanoscale features also necessarily lead to large low-frequency noise, due to the low number of charge carriers present in any nanowire device [6]. This low-frequency noise typically has a $1/f$ spectrum, whose magnitude scales with the inverse of the number of charge carriers, as empirically described by Hooge [7]. This large noise power spectral density (PSD) at low frequencies has been previously observed in many nanowire devices, including those fabricated from carbon nanotubes [8–10], silicon nanowires [11,12] and ZnO nanowires [13]. Low-frequency noise is particularly influential on the signal-to-noise ratio (SNR) of chemical sensors, due to the slow sensor dynamics seen in many devices. Low frequency components of $1/f$ noise can further lead to large drifts in the signal baseline between measurements, preventing long-term sensor calibration. It is thus desirable to track the nanowire sensor response in a way that reduces the influence of $1/f$ noise. One such technique is measuring the transient response of a sensor to gas exposure [14,15]. The specific transient signal of interest to this work is the initial-slope of the sensor transient, when a desorbed surface is exposed to an analyte.

Here we present a theoretical analysis of the SNR, dynamic range and response time of such a transient sensing scheme where the initial-slope of the sensor transient is measured. These theoretical results are illustrated with data acquired from suspended carbon nanotube field-effect transistor (CNTFET) nitrogen dioxide sensors, in order to characterize the relative performance of initial-slope and quasi-steady-state sensing in fabricated devices. These sensors are of particular interest because NO_2 is a common air pollutant which has been shown to have significant impacts on human health [16]. Previous work has demonstrated the response of CNT devices to NO_2 exposure [1,17–20]. Devices which were additionally functionalized with polymers have been shown to have sensitivities allowing for detection of NO_2 concentrations below 1 ppb [19]. Further work has demonstrated that decoration with Pt nanoparticles can allow for selective detection of NO_2 at room-

* Corresponding author at: Electrical Engineering and Computer Science, Massachusetts Institute of Technology, 77 Massachusetts Ave., Cambridge, MA 02139, USA.
E-mail address: psatt@mit.edu (P.F. Satterthwaite).

https://doi.org/10.1016/j.snb.2019.126674
Received 22 January 2019; Received in revised form 21 May 2019; Accepted 7 June 2019
Available online 21 June 2019

temperature [21], with similar selectivity enhancements being demonstrated for modified reduced graphene oxide sensors [22–25]. The experimental data from CNTFET NO_2 sensors presented in this work are analyzed in the context of the derived theoretical results, to compare the response time and linearity of the initial-slope sensing scheme with a more typical quasi-steady-state sensing scheme. Monte Carlo simulations are performed to assess the effect of $1/f$ noise on sensor calibration in a practical system, where calibration must be maintained over several months.

2. Theoretical analysis

2.1. Signal estimation in the presence of 1/f noise

Though a detailed description of the adsorption behavior of analytes on solid-state chemical sensors is in general complex, certain phenomenological behaviors are common to many sensor-analyte systems. When a fully desorbed chemical sensor surface is exposed to an analyte, the signal, $S(t)$, can often be described as a rising exponential. Mathematically this can be expressed,

$$S(t) = S_{ss}(p)(1 - e^{-t/\tau(p)}) \tag{1}$$

where p is the partial pressure/concentration of the analyte, $\tau(p)$ is the exponential time constant as a function of pressure and $S_{ss}(p)$ is the steady-state signal as a function of pressure.

Most sensor system architectures sample the steady-state signal, $S_{ss}(p)$. This signal can be simply tracked, however because it is a quasi-DC signal, low-frequency components of $1/f$ noise significantly degrade the SNR. Another disadvantage of tracking this signal is that many isotherms describing monolayer adsorption, including the Langmuir, Toth and Tempkin isotherms, exhibit saturation behavior [26]. This saturation occurs when the isotherm flattens out at high analyte concentrations, meaning surface adsorption is only weakly dependent on analyte concentration, reducing sensor sensitivity in this regime [26]. In practice, this reduction in sensitivity sets an upper limit on the dynamic range of the sensor. Further, tracking the steady-state behavior of the sensor requires waiting for the transient to settle. For a rising exponential, a time interval of $> 5\tau$ is required for the signal to settle within 1% of its final value, leading to a long response time. Though such a signal only represents an approximation of the steady-state signal, it will henceforth be referred to as the steady-state signal.

Due to the disadvantages of using the steady-state signal, it is desirable to use a signal that does not require a long stabilization time and is less sensitive to low-frequency noise. One such signal is the initial-slope of the sensor transient,

$$S_0' = \frac{\mathrm{dS}(t)}{\mathrm{dt}}\Big|_{t=0} = \frac{S_{ss}(p)}{\tau(p)} \tag{2}$$

Tracking this signal necessarily reduces response time, because it must be measured during the initial part of the sensor transient, without waiting for the transient to settle. Further, many simple implementations exist for tracking this signal, such as a linear least-squares fit to measured data.

The effect of $1/f$ noise on the steady-state and initial-slope signals can be calculated by determining the variance of the estimates of those signals in the presence of $1/f$ noise. The steady-state signal can be estimated by averaging N equally spaced samples of the device signal, $S(t)$. The output of this routine, $\hat{S}_{ss}$, can be expressed as:

$$\hat{S}_{ss} = \frac{1}{N}\sum_{i=1}^{N} S(i\Delta t) \tag{3}$$

where Δt is the spacing between samples. To estimate the initial-slope, S_0', a linear least-squares algorithm can be employed. Again using N samples equally spaced by Δt, the estimated slope, $\hat{S}_0'$, can be written as follows:

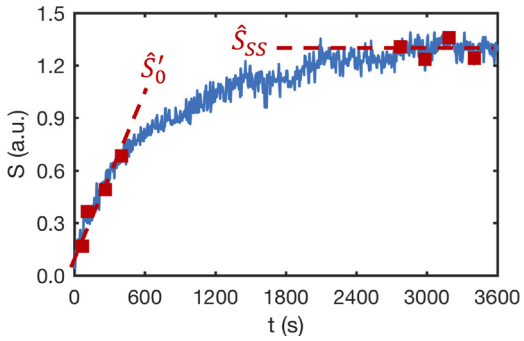

Fig. 1. Schematic illustration of sensor signal definitions: initial-slope ($\hat{S}_0'$) and steady-state ($\hat{S}_{ss}$) signals with $N = 4$, applied to raw sensor output.

$$\hat{S}_0' = \frac{\sum_{i=1}^{N} 6S(i\Delta t)[2i - (N+1)]}{\Delta t N(N^2-1)} \tag{4}$$

The derivation of Eq. (4) is presented in Appendix A. A schematic illustration of these sensor signal definitions, as applied to a sensor signal with $1/f$ noise is presented in Fig. 1.

Calculating the variances of $\hat{S}_{ss}$ and $\hat{S}_0'$ is challenging in the presence of $1/f$ noise. The self-similar behavior of $1/f$ noise leads to strong correlations across all time scales, meaning that variances and correlations are only well defined with respect to a given observation window [27,6]. This stands in contrast to white noise, where the measured variance is independent of the observation window. Based on the methodology in [28], this work will model $1/f$ noise with a correlated random variable, which given a fixed observation window, has a well defined variance, σ_f^2, and autocorrelation, $R(\tau)$. Given this observation window, the normalized autocorrelation can be approximately written [28,29]:

$$R(\tau) = \begin{cases} 1 & \tau = 0 \\ -k\ln|\tau/\tau_l| & 0 < |\tau| < \tau_l \\ 0 & |\tau| > \tau_l \end{cases} \tag{5}$$

where τ is the temporal delay between two samples, k is a constant proportional to the power spectral density (PSD) of the $1/f$ noise and τ_l defines the timescale over which the correlations between samples affect the measurement. τ_l is necessarily larger than the observation window, if the noise has a $1/f$ spectrum across all measured frequencies.

In order to simplify further analysis, the autocorrelation can be approximated by its series expansion about a representative time in the acquisition window, $t_{rep} < t_{acq}$, where $t_{acq} = N\Delta t$ is the measurement acquisition time (See Eqs. (3, 4)). Under this approximation, the autocorrelation function can be written as

$$R(\tau) \approx R(t_{\mathrm{rep}}) - |\tau - t_{\mathrm{rep}}|*\frac{\partial R(\tau)}{\partial \tau}\Big|_{\tau=t_{\mathrm{rep}}} = R_0 - \frac{k}{t_{\mathrm{rep}}}|\tau| \tag{6}$$

where $R_0 = k(1 - \ln(t_{rep}/\tau_l))$. The autocorrelation function of a signal with a $1/f$ noise spectrum is presented in Fig. 2, in addition to a fitted function of the same form as Eq. (5), and its linear approximation.

Under the linear approximation (Eq. (6)), the variance of the steady-state ($\hat{S}_{ss}$) and initial-slope ($\hat{S}_0'$) estimators can be calculated, using the identity $\mathrm{Var}[\Sigma_i c_i X_i] = \Sigma_{i,j} c_i c_j \mathrm{Cov}[X_i, X_j]$ where the c_i are constants and X_i are random variables. Using this approximated autocorrelation function, the variance of the steady-state estimator can be evaluated under the assumption that $N >> 1$. Detailed derivation of this variance is provided in Appendix A. This analysis results in the following expression for steady-state variance:

$$\mathrm{Var}[\hat{S}_{ss}] = \sigma_f^2\left(\frac{1}{N} + R_0 - \frac{1}{3}\frac{t_{\mathrm{acq}}}{t_{\mathrm{rep}}}k\right) \tag{7}$$

Where σ_f, R_0 and k are the previously introduced quantities describing

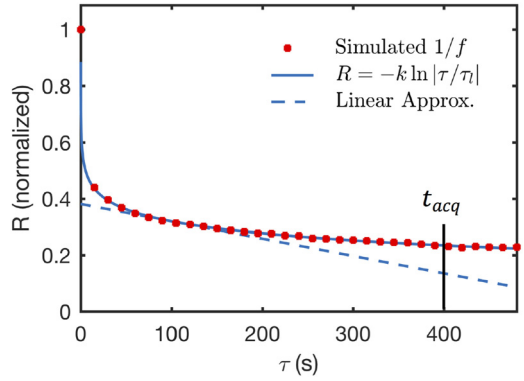

Fig. 2. Normalized autocorrelation function. Red data points represent autocorrelation function calculated from noise with $1/f$ PSD. Solid blue line shows fitted function of the form $R(\tau) = -k\ln|\tau/\tau_l|$. Dashed blue line shows series expansion of fitted function around $t_{rep} = t_{acq}/4$ where $t_{acq} = 400$ s here.

the $1/f$ noise. This expression can be compared to that for uncorrelated, white noise, where R_0, $k = 0$. For white noise $\mathrm{Var}[\hat{S}_{ss}] = \sigma_f^2/N$.

The variance of the initial-slope estimator is also derived in Appendix A. Again assuming that $N >> 1$, this variance is shown to be:

$$\mathrm{Var}[\hat{S}_0'] = 12\left(\frac{\sigma_f}{t_{acq}}\right)^2\left(\frac{1-R_0}{N} + \frac{1}{5}\frac{t_{acq}}{t_{rep}}k\right) \tag{8}$$

A similar expression can again be derived for white noise by setting R_0, $k = 0$, yielding $\mathrm{Var}[\hat{S}_0'] = (\sigma_f/t_{acq})^2(12/N)$.

Both Eq. (7) and (8) can be further simplified in the limit where $N >> 1/k$, and $\tau_l >> t_{acq}$, yielding more useful forms. It was empirically determined that the linear approximation in Eq. (6) accurately represents Eq. (5) when $t_{rep} = t_{acq}/4$ (see Appendix A). Using this value, the variance of the steady-state and transient signals are respectively given by

$$\mathrm{Var}[\hat{S}_{ss}] \approx \sigma_f^2 k \ln\left(4\frac{\tau_l}{t_{acq}}\right) \tag{9}$$

$$\mathrm{Var}[\hat{S}_0'] \approx \frac{48}{5}\left(\frac{\sigma_f}{t_{acq}}\right)^2 k \tag{10}$$

Eqs. (9) and (10) make clear the effect of the correlated nature of $1/f$ noise. The correlated nature of the noise fundamentally limits the minimum achievable variances to be proportional to k, a constant describing the PSD of the noise. This fundamental limit is particularly important in nanowire devices because k is large due to the scaling of noise amplitude with the inverse of the number of charge carriers [7].

Further, in the large N limit, the variance of the transient estimator is insensitive to the low frequency cutoff of the noise, τ_l. This insensitivity occurs because very low frequency components of the noise do not influence the estimated slope, as they are approximately constant across any given measurement of the slope. These low frequency components do however introduce an offset to the signal which varies between measurements, and greatly affects the steady-state estimator. The insensitivity of the initial-slope signal to low-frequency components of noise is particularly important in practical applications where the sensor must remain well calibrated over timescales ranging from months to years. Because drifts in the baseline grow logarithmically with time [28], without proper drift compensation the error it introduces will eventually overwhelm the steady-state signal. For example, when the acquisition time is on the order of seconds, and the time scale over which the sensor must be calibrated is on the order of one month, the quantity $\ln(4\tau_l/t_{acq})$ increases the noise by a factor of 16 for the steady-state signal, without effecting the initial-slope signal.

To quantitatively compare the SNR of the steady-state and initial-slope sensing schemes, the root-mean-squared error (σ_{RMS}) of the estimated pressure relative to its true value can be calculated. This value is calculated for the steady-state and initial-slope signals respectively using:

$$\sigma_{\mathrm{RMS,ss}} = \left(\frac{\mathrm{dS_{ss}}(p)}{\mathrm{dp}}\right)^{-1}\sqrt{\mathrm{Var}[\hat{S}_{ss}]} \tag{11}$$

$$\sigma_{\mathrm{RMS,tran}} = \left(\frac{\mathrm{dS_0'}(p)}{\mathrm{dp}}\right)^{-1}\sqrt{\mathrm{Var}[\hat{S}_0']} \tag{12}$$

where $dS_{ss}(p)/dp$ and $\mathrm{dS_0'}(p)/\mathrm{dp}$ are the sensitivities of the steady-state and initial-slope signals respectively. The following section will compare these calculated RMS errors for the case of a device described by a Langmuir isotherm.

2.2. Application to the Langmuir isotherm

The Langmuir adsorption model describes the adsorption/desorption behavior of analytes on many solid-state chemical sensors, including CNTFET gas-sensors [18,30–33]. In this model, under the assumption of zero adsorbed molecules at $t = 0$, the dynamics of the surface coverage (θ) are given by [26]:

$$\theta(t) = \frac{K_{\mathrm{ads}}p}{K_{\mathrm{ads}}p + K_{\mathrm{des}}}\left(1 - e^{-(K_{\mathrm{ads}}p + K_{\mathrm{des}})t}\right) \tag{13}$$

Here K_{ads} and K_{des} are the adsorption and desorption coefficients respectively, and p is the concentration/partial-pressure of the analyte. The steady-state behavior of this system is described by the well known Langmuir isotherm,

$$\theta_{\mathrm{ss}}(p) = \frac{K_{\mathrm{ads}}p}{K_{\mathrm{ads}}p + K_{\mathrm{des}}} \tag{14}$$

Under the same initial conditions, the initial-slope signal can be simply written,

$$\frac{d\theta(t)}{\mathrm{dt}}\Big|_{t=0} = K_{\mathrm{ads}}p \tag{15}$$

This expression highlights an important advantage of the initial-slope signal. In Langmuir systems, the initial-slope is linearly proportional to the analyte concentration, in contrast to the highly non-linear steady-state behavior of the Langmuir isotherm, which shows saturation at high analyte concentrations. This means that initial-slope sensing has the potential to operate at higher concentrations beyond the dynamic range available to steady-state sensing. Further, measurement of this signal does not require waiting for the device to stabilize, necessarily reducing the sensor response time.

The sensitivity of the steady-state and initial-slope signals can also be calculated from Eq. (13). Assuming a linear proportionality of α between surface coverage, θ, and the measured signal, S, the following sensitivities are derived from differentiating Eq. (13) with respect to analyte concentration:

$$\frac{\mathrm{dS_{ss}}}{\mathrm{dp}} = \frac{\alpha K_{\mathrm{ads}}K_{\mathrm{des}}}{(K_{\mathrm{ads}}p + K_{\mathrm{des}})^2} \tag{16}$$

$$\frac{\mathrm{dS_0'}}{\mathrm{dp}} = \alpha K_{\mathrm{ads}} \tag{17}$$

Eq. (16) demonstrates the non-linearity of the steady-state sensitivity due to the saturation behavior of the Langmuir isotherm, in contrast to the linear initial-slope signal in Eq. (17), indicating that the initial-slope signal has the potential for a larger dynamic range. These sensitivities can be combined with Eqs. (11) and (12) to calculate the respective RMS errors for initial-slope and steady-state sensing, allowing the following inequality to be constructed for the conditions when initial-slope sensing has a higher SNR than steady-state sensing:

$$t_{acq} > \frac{1}{K_{des}\left(1+\frac{K_{ads}}{K_{des}}p\right)^2}\sqrt{\frac{48}{5\ln(4\tau_l/t_{acq})}} \quad (18)$$

This inequality is derived from the previous equations with the assumption that $N >> 1/k$. Eqn. (18) elucidates that initial-slope sensing has lower RMS error than steady-state sensing when τ_l is large relative to t_{acq} (drift is poorly compensated) and when $p >> K_{des}/K_{ads}$. This demonstrates that transient sensing has better noise performance in the regimes where steady-state sensing is most limited, when p is large, and when low-frequency components of noise dominate. In order to understand the relative performance of these two sensing schemes in realized devices, measurements of CNTFET NO_2 sensors were performed.

3. Methods

3.1. Device fabrication

Suspended CNTFET sensors were fabricated using a dry-transfer technique, detailed by Mouth et al. [34]. Subsequent to growth, single-walled CNTs (SWCNTs) were transferred to a receiving substrate using a micromanipulator. Prior to CNT transfer, support structures for the suspended CNT sensors were fabricated from micromachined silicon-dioxide, as detailed in [35]. Gate, source and drain electrodes were fabricated from evaporated 0.5 nm/40 nm Cr/Pd. A scanning electron microscope (SEM) image and schematic illustration of the fabricated CNTFET sensors are presented in Fig. 3a and b respectively.

Subsequent to transfer, a bias was applied across the source-drain electrodes. By measurement of the resulting current, semiconducting SWCNTs could be post-selected. The data presented in this work are from three devices. All measurements in this paper are from devices with a gate pitch of ~2.2 μm (see Fig. 3b), and a 1.8 μm gap between the suspended CNT channel and the gate electrode.

3.2. Gas sensing measurements

Measurements of gas-sensing performance were conducted at atmospheric pressure in a home-built gas measurement setup. A constant flow of synthetic dry air was maintained over the substrate throughout the measurement process. The measured devices were exposed to NO_2 concentrations ranging from 0 to 10 ppm. Transfer characteristics were recorded using a pulsed measurement scheme described in [36]. V_{SD} and V_{GS} were generated using a National Instruments DAQ card (NI PCI-6289). The resulting I_D was amplified by a low noise current-to-voltage amplifier (Femto DHPCA 100), and the signal was fed-back into the DAQ card. Heating of the devices was accomplished with a Joule heater integrated into the measurement circuit-board. The temperature of the heater during the heating cycle was measured to be 120° C. The corresponding temperature of the device substrate is estimated from IR thermometry to be ~70° C. Previous work has demonstrated a reduction in desorption time from over 12 hours to under 10 min via self-heating, under similar heating conditions [18].

3.3. Monte-Carlo simulation

Monte Carlo simulations were preformed in MATLAB using simulated $1/f$ noise. $1/f$ noise was generated from pseudo-random white-noise which was filtered in the Fourier domain. This noise was verified to have a $1/f$ spectrum down to 10^{-7} Hz (1/100 days). The magnitude of this spectrum was normalized such that the variance of the noise signal when calculated across a certain bandwidth, was the same as the variance in a CNTFET device, as measured across the same bandwidth.

In order to asses the RMS error associated with sensing a given concentration, 500 gas sensing events were simulated at each concentration. Each gas sensing event was combined with a random noise sample drawn from the simulated $1/f$ noise signal. During each gas sensing event, the initial-slope and steady-state behavior of a signal with the following form was measured:

$$V_{TH}(t) = \Delta V_{TH,SS}\frac{K_{ads}p}{K_{ads}p + K_{des}}(1 - e^{-(K_{ads}p+K_{des})t}) + \epsilon(t) \quad (19)$$

Where $\Delta V_{TH,SS}$ is the threshold voltage shift at full surface coverage ($\theta = 1$). The parameters for this expression were the experimental parameters of a CNTFET gas sensor, as described in the subsequent section. $\epsilon(t)$ represents the added noise. The variance of the simulated initial-slope and transient signals was used to determine the corresponding RMS error in measured gas concentration through the sensitivities given in Eqs. (16) and (17). The experiment was repeated with a white-noise signal, that had the same variance as the $1/f$ noise, to asses the effect of correlated noise on the signal.

4. Results and discussion

4.1. Transient measurement of CNTFET NO_2 sensor

To characterize the transient response of fabricated CNTFET gas sensors, time-resolved measurements of the sensors in dry synthetic air atmospheres with varied NO_2 concentrations were performed. These suspended CNTFET sensors have previously been shown to provide a unique combination of high sensitivity [17], low hysteresis [37], and ultra-low power operation [18].

Fig. 3c shows the transfer characteristics of a typical CNTFET sensor in both synthetic dry air and NO_2 atmospheres. These data demonstrate the differing responses to gas exposure which have been observed for CNTFET sensors: (1) shift in threshold voltage, (2) tilt of transfer characteristic and (3) increase in on-state current. These different responses correspond to gas adsorption on the CNT channel for (1), and

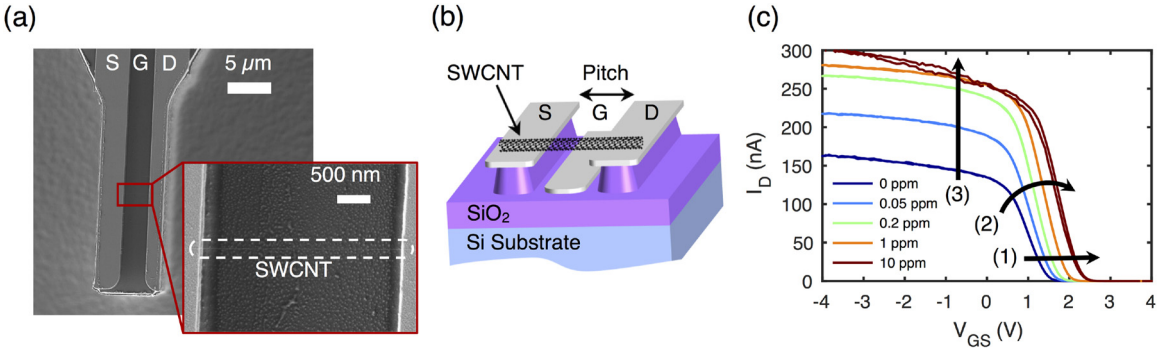

Fig. 3. (a) SEM image of suspended CNTFET device (b) Schematic illustration of suspended CNTFET device (c) Typical transfer characteristic at $V_{SD} = 500mV$. Different traces represent different NO_2 concentrations. These data show **(1)** a shift in the threshold voltage **(2)** tilt of transfer characteristic **(3)** increased saturation current.

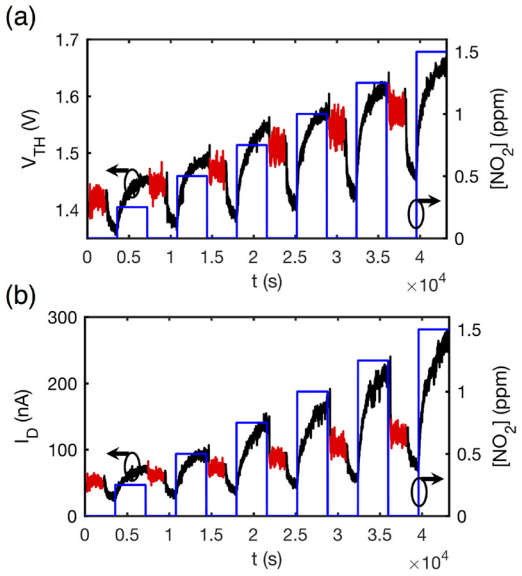

Fig. 4. Transient response of desorbed sensor to increasing NO_2 concentrations. (a) Threshold voltage detection scheme (I_D = 50 nA/V_{SD} = 500 mV). (b) Saturation current detection scheme (V_{GS} = -1.4 V/V_{SD} = 500 mV). Red sections of traces represent time when heating is applied to reset the surface, blue traces plotted in the right y-axis represent applied gas concentration.

adsorption on the contact regions for (2,3) [38]. Transient measurements of both threshold voltage shifts and on-state current modulation were performed to verify that both responses can be used to track the steady-state and initial-slope signal.

These measurements are presented in Fig. 4, which shows transient measurements where 1-hour long NO_2 gas pulses were alternated with 1-hour long desorption periods where no NO_2 is present. A concentration range of 0.25-1.5 ppm was chosen in order to observe the full Langmuir isotherm and accurately estimate adsorption parameters. Measurements of device transfer characteristics were recorded every 5 seconds. Fig. 4a shows the threshold voltages, here defined as the gate voltage needed to reach a given threshold current (50 nA for this device) [39], extracted from this measurement. Fig. 4b shows the saturation current measured at $V_{GS} = -1.4$ V, from the same experiment. During the periods indicated in Fig. 4 in red, the sample was heated by an external Joule heater to allow for sensor reset via thermally induced desorption [18]. The data in Fig. 4 demonstrate sensor recovery under external heating, as well as an increased initial-slope and steady-state signal at higher NO_2 concentrations, consistent with the Langmuir model. The slowly decaying signal observed subsequent to applied heating is attributed to the slow thermal time constant of the test chamber. These data also show a drift in the sensor baseline, common to CNTFET devices. These measurements do not allow conclusive determination of whether this drift is due to sensor degradation, imperfect desorption or low frequency $1/f$ noise. It is argued in Appendix A that imperfect desorption will not significantly affect the measured initial-slope, or steady-state signal.

The data in Fig. 4 demonstrate that both the threshold voltage and saturation current detection schemes show an increase in the initial-slope and steady-state signal as analyte concentration increases. Due to the different kinetics of the adsorption of NO_2 on the CNT channel and metal contact regions, these signals will in general have different Langmuir isotherms, and consequentially transient behavior. Subsequent analysis in this work will focus on the threshold voltage signal, though both signals could be used to sense gas concentration. At each concentration step, the threshold voltage signal was fitted to a rising exponential, $V_{TH}(t) = V_0 + \Delta V_{TH,SS}(1 - \exp(-t/\tau))$. From this fitted exponential, the steady-state signal, ($\Delta V_{TH,SS}$), and initial-slope ($\Delta V_{TH,SS}/\tau$) as a function of NO_2 concentration were extracted. These data are presented as the black data points in Fig. 5, with the error-bars representing the 95% confidence intervals for the fitted parameters due to the presence of noise.

The steady-state and initial-slope data in Fig. 5a and b are well modeled by a Langmuir isotherm, and linear fit respectively, consistent with a Langmuir adsorption model. These data thus verify the linearity of the initial-slope signal relative to the steady-state signal. From the fitted isotherm and initial-slope, the adsorption coefficients were extracted. The extracted values, $1/K_{ads}$ = 116 s·Pa and $1/K_{des}$ = 2200 s are consistent with previous reports [18].

4.2. Noise performance of CNTFET sensors

The standard deviation of the extracted threshold voltage signal for the device presented in Figs. 4 and 5 was measured to be 5.1 mV at 50 nA drain current, for a 125 s observation window. Noise spectral characterization of a different device was additionally performed. Time-domain measurements of steady-state current at a fixed voltage bias were taken in both synthetic dry air and varying NO_2 atmospheres. Fourier analysis of these measurements is presented in Fig. 6. Under all measurement conditions, the PSD is well modeled by a $1/f$ dependency, for f = 0.5–500 Hz. The noise PSD was observed to be primarily dependent on bias current, with only a weak dependency on gas concentration. The observation of the same spectral shape for both synthetic dry air and NO_2 atmospheres indicates that measurement of the

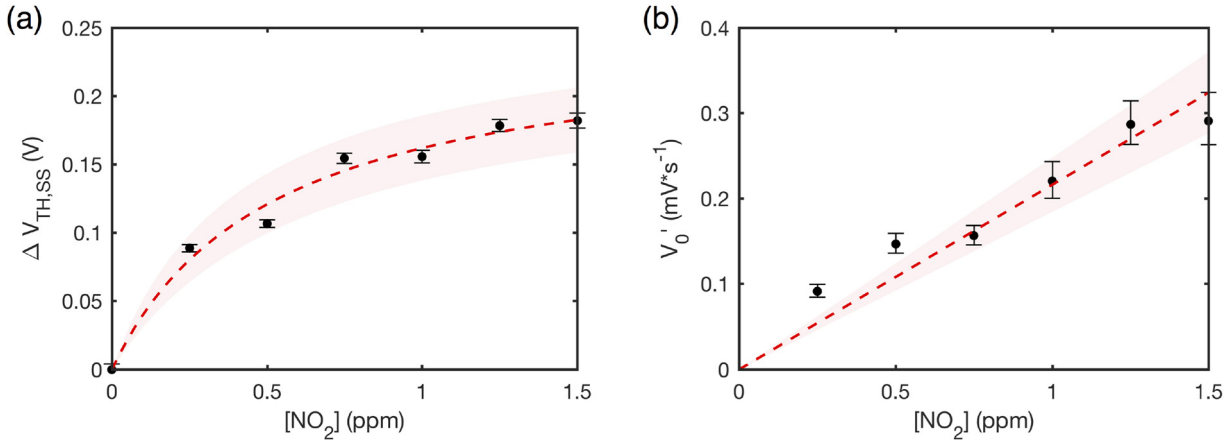

Fig. 5. Fitted steady-state and transient parameters for threshold voltage shifts at I_D = 50 nA/V_{SD} = 500 mV. **(a)** steady-state change in V_{GD} and fitted Langmuir isotherm. **(b)** initial-slope of transient and fitted linear dependency on gas concentration. Shaded pink areas, and error bars on data points represent 95% confidence intervals for the fitted parameters.

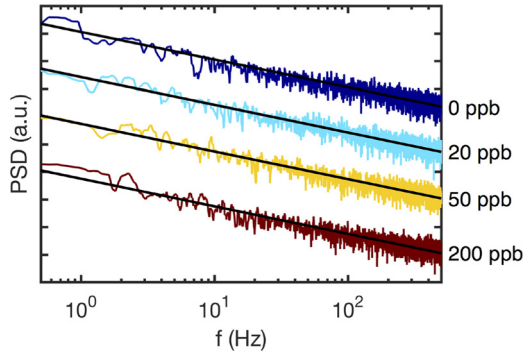

Fig. 6. Measured power spectral density of CNTFET sensor. Device was biased at $V_{GS} = -2.0$ V/$V_{SD} = 500$ mV. Black lines represent fitted $1/f$ function. Spectra are offset for clarity. y-axis represents arbitrary units on a logarithmic scale.

noise spectrum cannot be used for selective detection of NO_2, in contrast to the work of Rumyantsev et al., where it was demonstrated that measurement of the noise spectra of graphene gas sensors can improve the selectivity in detecting volatile organic compounds [40].

Fig. 7a presents Monte-Carlo simulations of the RMS error of measurements made using a sensor that has the same parameters as the device presented in Figs. 4 and 5 . A concentration range of 0-150 ppb is considered, due to the relevance of these concentrations to human health [16,41]. The markers represent the RMS error of 500 simulated measurements of gas concentration using a steady-state (blue) and an initial-slope (red) sensing scheme, taken at random times over the course of 100 days. These conditions represent a realistic field deployment of the sensor, that are however difficult to replicate in a lab environment. The simulated measurements in Fig. 7a assume $N = 100$ and $t_{acq} = 400$ s. To illustrate the effect of $1/f$ noise, sensing in the presence of white noise (triangular markers) and noise with a $1/f$ spectrum down to 10^{-7} Hz (1/100 days, square markers) is compared. The solid and dashed lines represent theoretical predictions for the RMS error in the presence of white and $1/f$ noise respectively, calculated using Eqs. (7) and (8). These theoretical predictions show strong agreement with Monte-Carlo simulations.

These results show that with current devices, initial-slope sensing has a higher RMS error across the entire concentration range of interest. Further, for $N = 100$, $1/f$ noise results in a significantly higher RMS error than white noise, for both steady-state and initial-slope sensing. Though initial-slope sensing has a higher RMS error than steady-state sensing, its response time is dramatically better. In the concentration range of 1-150 ppb, the exponential time constant of the sensor varies from 1700 s to 2200 s, meaning that it will take over an hour for the transient to settle within 10% of its final value (more than two hours are needed to settle within 1%). This long waiting time stands in stark contrast to the 400 s needed to acquire the transient signal.

The response times and relative sensitivities of the two detection schemes can by changed by increasing the adsorption coefficient. Previous work has shown that functionalization with a variety of agents ranging from organic polymers to metallic nanoclusters can increase the adsorption coefficient by up to two orders of magnitude [19–21], improving both sensitivity and selectivity. The effect on SNR of increasing the measured adsorption coefficient by 50×, well within experimentally demonstrated values, is now considered, for both steady-state and initial-slope sensing. Noise analysis of such a device is presented in Fig. 7b, with t_{acq} reduced to 40 s due to the reduced time constants present in the functionalized system (140-2000 s).

Here, we observe that initial-slope sensing has a constant RMS error of ~12 ppb across the concentration range of interest. In contrast, steady-state sensing has a lower error at low concentrations, consistent with previous reports of sub-ppb detection [19], however the error diverges at high concentrations due to the flattening out of the Langmuir isotherm. Though steady-state sensing is more sensitive at low concentrations, it will still have a slow response time (~2000 s), because previously demonstrated functionalization techniques do not increase desorption rate [19,20]. Thus, if functionalization is pursued, initial-slope sensing is expected to have a higher SNR across the sensing range of interest, in addition to its advantages in terms of increased linearity and lowered response time.

5. Conclusions

A systematic comparison of the performance metrics of initial-slope and steady-state sensing has been performed. It is demonstrated that relative to steady-state sensing, initial-slope sensing lowers response time, and can lead to better linearity and dynamic range, due to the flattening out of the Langmuir isotherm. Conditions under which initial-slope sensing leads to higher SNR have been derived. These results, combined with measurements of pristine CNTFET NO_2 sensors allow us to conclude that with current unfunctionalized devices initial-slope sensing will not benefit sensing applications where maximizing SNR is the key criterion. In applications where response time is a key

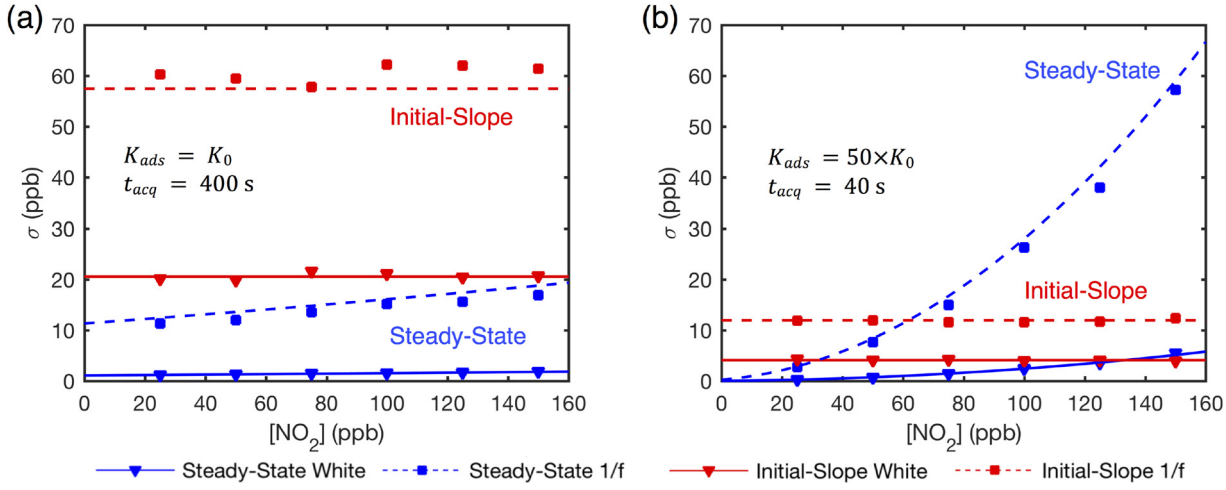

Fig. 7. Monte-Carlo simulations of error of NO_2 readings from device with same parameters as **(a)** Measured sample with $N = 100$, $t_{acq} = 400$ s, $1/K_{ads} = 1/K_0 = 116$ s·Pa **(b)** Same sample, if K_{ads} is increased by 50×, with $N = 100$, $t_{acq} = 40$ s. Triangular markers represent simulated RMS error assuming white PSD, square markers represent simulated RMS error assuming $1/f$ PSD. Blue traces are from steady-state sensing, red traces from transient sensing. Solid and dashed lines represent theoretical prediction of RMS error in the presence of white and $1/f$ noise respectively.

performance metric the initial-slope sensing scheme will, however, be preferred. Functionalization of CNTFET NO_2 sensors can lower response times further, and change the relative SNR of the two sensing schemes.

Though the experimental results presented here were acquired in a laboratory environment where gas flow could be controlled, the sensing schemes described in this work are applicable to many sensing environments. The initial-slope sensing scheme simply requires that: (1) sensor reset can be achieved, with the transition between reset and sensing mode occurring quickly relative to the adsorption time constant, and (2) the analyte concentration is approximately constant across the acquisition window. This second requirement can be relaxed by controlling the flow of gas into the measurement chamber. These requirements are readily fulfilled when using CNTFET devices are used as environmental NO_2 sensors. Reset to a desorbed state where the sensor is prepared for a new sensing cycle can be achieved through both thermal and UV methods [18,42,19]. Further, the relevant timescale for change in environmental NO_2 is on the order of one hour, long relative to the ~5 min. acquisition windows considered here [43–45]. Practical application of the initial-slope sensing scheme is further possible due to the simplicity of the least-squares algorithm described in Eq. (4), which can be implemented on compact hardware.

Though the results of this work focus on CNTFET NO_2 sensors, they can provide useful criteria towards the design of other chemical and biological sensing systems, due to the minimal requirements for implementing an initial-slope sensing routine, and due to the ubiquity of low-frequency noise and Langmuir kinetics which limit these systems [46–48]

Author contributions

P.F.S. and C.R. conducted theoretical analysis. S.E. fabricated all measured devices. P.F.S. conducted measurements presented in Figs. 3–5 with help from S.E. S.N. conducted the measurement presented in Fig. 6. P.F.S. conducted the Monte Carlo simulations. C.H. supervised this project. All authors contributed to the design of experiments. P.F.S. primarily wrote the manuscript with contributions from all authors.

Notes

The authors declare no competing financial interest.

Acknowledgements

The authors acknowledge financial support from SNF-FLAG ERA CONVERGENCE (20FE-1_170224) “Frictionless Energy Efficient Convergent Wearables for Healthcare and Lifestyle Applications.” P.F.S. acknowledges financial support from the Stanford Global Studies Internship Program during the summer of 2017. The authors thank Miroslav Haluska, Laura Jenni and Lalit Kumar for helpful discussion.

Appendix A. Supplementary Data

Supplementary data associated with this article can be found, in the online version, at doi:https://doi.org/10.1016/j.snb.2019.126674.

References

[1] J. Kong, N. Franklin, C. Zhou, M. Chapline, S. Peng, K. Cho, H. Dai, Nanotubes molecular wires as chemical sensors, Science 287 (2000) (2000) 622–625, https://doi.org/10.1126/science.287.5453.622.
[2] Y. Cui, Nanowire nanosensors for highly sensitive and selective detection of biological and chemical species, Science 293 (5533) (2001) 1289–1292, https://doi.org/10.1126/science.1062711.
[3] X.-J. Huang, Y.-K. Choi, Chemical sensors based on nanostructured materials, Sens. Actuators B: Chem. 122 (2007) 659–671, https://doi.org/10.1016/j.snb.2006.06.022.
[4] F. Patolsky, G. Zheng, C.M. Lieber, Nanowire sensors for medicine and the life sciences, Nanomedicine 1 (1) (2006) 51–65, https://doi.org/10.2217/17435889.1.1.51.
[5] D.R. Kauffman, A. Star, Carbon nanotube gas and vapor sensors, Angew. Chem. Int. Ed. 47 (35) (2008) 6550–6570, https://doi.org/10.1002/anie.200704488.
[6] S. Kogan, Electronic Noise and Fluctuations in Solids, Cambridge University Press, 2008.
[7] F. Hooge, 1/f noise is no surface effect, Phys. Lett. A 29 (3) (1969) 139–140, https://doi.org/10.1016/0375-9601(69)90076-0.
[8] E.S. Snow, J.P. Novak, M.D. Lay, F.K. Perkins, 1/f noise in single-walled carbon nanotube devices, Appl. Phys. Lett. 85 (18) (2004) 4172–4174, https://doi.org/10.1063/1.1812838.
[9] Y.-M. Lin, J. Appenzeller, J. Knoch, Z. Chen, P. Avouris, Low-frequency current fluctuations in individual semiconducting single-wall carbon nanotubes, Nano Lett. 6 (5) (2006) 930–936, https://doi.org/10.1021/nl052528d.
[10] M. Ishigami, J.H. Chen, E.D. Williams, D. Tobias, Y.F. Chen, M.S. Fuhrer, Hooge's constant for carbon nanotube field effect transistors, Appl. Phys. Lett. 88 (20) (2006), https://doi.org/10.1063/1.2206685.
[11] K. Bedner, V.A. Guzenko, A. Tarasov, M. Wipf, R.L. Stoop, S. Rigante, J. Brunner, W. Fu, C. David, M. Calame, J. Gobrecht, C. Schönenberger, Investigation of the dominant 1/f noise source in silicon nanowire sensors, Sens. Actuators B: Chem. 191 (2014) 270–275, https://doi.org/10.1016/j.snb.2013.09.112.
[12] N.K. Rajan, D.A. Routenberg, J. Chen, M.A. Reed, 1/f noise of silicon nanowire BioFETs, IEEE Electron Device Lett. 31 (6) (2010) 615–617, https://doi.org/10.1109/LED.2010.2047000.
[13] S. Ju, S. Kim, S. Mohammadi, D.B. Janes, Y.-G. Ha, A. Facchetti, T.J. Marks, Interface studies of ZnO nanowire transistors using low-frequency noise and temperature-dependent I-V measurements, Appl. Phys. Lett. 92 (2) (2008) 022104, https://doi.org/10.1063/1.2830005.
[14] T. Eklöv, P. Mårtensson, I. Lundström, Enhanced selectivity of MOSFET gas sensors by systematical analysis of transient parameters, Analytica Chim. Acta 353 (2-3) (1997) 291–300, https://doi.org/10.1016/S0003-2670(97)87788-4.
[15] A. Hierlemann, R. Gutierrez-Osuna, Higher-order chemical sensing, Chem. Rev. 108 (2) (2008) 563–613, https://doi.org/10.1021/cr068116m.
[16] U. Latza, S. Gerdes, X. Baur, Effects of nitrogen dioxide on human health: Systematic review of experimental and epidemiological studies conducted between 2002 and 2006, Int. J. Hygiene Environ. Health 212 (3) (2009) 271–287, https://doi.org/10.1016/j.ijheh.2008.06.003.
[17] M. Mattmann, T. Helbling, L. Durrer, C. Roman, C. Hierold, R. Pohle, M. Fleischer, Sub-ppm NO2 detection by Al2O3 contact passivated carbon nanotube field effect transistors, Appl. Phys. Lett. 94 (18) (2009) 183502, https://doi.org/10.1063/1.3125259.
[18] K. Chikkadi, M. Muoth, V. Maiwald, C. Roman, C. Hierold, Ultra-low power operation of self-heated, suspended carbon nanotube gas sensors, Appl. Phys. Lett. 103 (22) (2013), https://doi.org/10.1063/1.4836415.
[19] P. Qi, O. Vermesh, M. Grecu, A. Javey, Q. Wang, H. Dai, S. Peng, K.J. Cho, Toward large arrays of multiplex functionalized carbon nanotube sensors for highly sensitive and selective molecular detection, Nano Lett. 3 (3) (2003) 347–351, https://doi.org/10.1021/nl034010k.
[20] M. Penza, G. Cassano, R. Rossi, M. Alvisi, A. Rizzo, M.A. Signore, T. Dikonimos, E. Serra, R. Giorgi, Enhancement of sensitivity in gas chemiresistors based on carbon nanotube surface functionalized with noble metal (Au, Pt) nanoclusters, Appl. Phys. Lett. 90 (17) (2007) 1–4, https://doi.org/10.1063/1.2722207.
[21] S.W. Choi, J. Kim, Y.T. Byun, Highly sensitive and selective NO2 detection by Pt nanoparticles-decorated single-walled carbon nanotubes and the underlying sensing mechanism, Sens. Actuators B: Chem. 238 (2) (2017) 1032–1042, https://doi.org/10.1016/j.snb.2016.07.153.
[22] W. Yuan, A. Liu, L. Huang, C. Li, G. Shi, High-performance NO 2 sensors based on chemically modified graphene, Adv. Mater. 25 (5) (2013) 766–771, https://doi.org/10.1002/adma.201203172.
[23] H. Zhang, J. Feng, T. Fei, S. Liu, T. Zhang, SnO2 nanoparticles-reduced graphene oxide nanocomposites for NO2 sensing at low operating temperature, Sens. Actuators B: Chem. 190 (2) (2014) 472–478, https://doi.org/10.1016/j.snb.2013.08.067.
[24] M. Shaik, V.K. Rao, M. Gupta, K.S. Murthy, R. Jain, Chemiresistive gas sensor for the sensitive detection of nitrogen dioxide based on nitrogen doped graphene nanosheets, RSC Adv. 6 (2) (2016) 1527–1534, https://doi.org/10.1039/c5ra21184k.
[25] S.W. Lee, W. Lee, Y. Hong, G. Lee, D.S. Yoon, Recent advances in carbon material-based NO2 gas sensors, Sensors and Actuators B: Chemical 255 (2) (2018) 1788–1804, https://doi.org/10.1016/j.snb.2017.08.203.
[26] R.I. Masel, Principles of Adsorption and Reaction on Solid Surfaces, 3rd Edition, John Wiley and Sons, 1996.
[27] B. Mandelbrot, Some noises with 1/f spectrum, a bridge between direct current and white noise, IEEE Trans. Information Theory 13 (2) (1967) 289–298, https://doi.org/10.1109/TIT.1967.1053992.
[28] M. Keshner, 1/f noise, Proc. IEEE 70 (3) (1982) 212–218, https://doi.org/10.1109/PROC.1982.12282.
[29] F. Vernotte, E. Lantz, Metrology and 1/f noise: linear regressions and confidence intervals in flicker noise context, Metrologia 52 (2) (2015) 222–237, https://doi.org/10.1088/0026-1394/52/2/222.
[30] Z.F. Li, F.D. Blum, M.F. Bertino, C.S. Kim, Understanding the response of nanostructured polyaniline gas sensors, Sens. Actuators B: Chem. (2013), https://doi.org/10.1016/j.snb.2013.03.125.
[31] R. McKendry, J. Zhang, Y. Arntz, T. Strunz, M. Hegner, H.P. Lang, M.K. Baller, U. Certa, E. Meyer, H.-J. Guntherodt, C. Gerber, Multiple label-free biodetection and quantitative DNA-binding assays on a nanomechanical cantilever array, Proc. Natl. Acad. Sci. (2002), https://doi.org/10.1073/pnas.152330199.

[32] D. Zhang, D. Wang, X. Zong, G. Dong, Y. Zhang, High-performance QCM humidity sensor based on graphene oxide/tin oxide/polyaniline ternary nanocomposite prepared by in-situ oxidative polymerization method, Sens. Actuators B: Chem. (2018), https://doi.org/10.1016/j.snb.2018.02.012.
[33] Y. Chen, A. Nguyen, L. Niu, R.M. Corn, Fabrication of DNA,microarrays with poly(L-glutamic acid) monolayers on gold substrates for SPR imaging measurements, Langmuir 25 (9) (2009) 5054–5060, https://doi.org/10.1021/la804021t.
[34] M. Muoth, C. Hierold, Transfer of carbon nanotubes onto microactuators for hysteresis-free transistors at low thermal budget, Proceedings of the IEEE International Conference on Micro Electro Mechanical Systems (MEMS) (February) (2012) 1352–1355, https://doi.org/10.1109/MEMSYS.2012.6170417.
[35] S. Eberle, C. Roman, C. Hierold, Effect of varying gate distance on the threshold voltage shift in carbon nanotube field effect transistor gas sensors, Microelectronic Eng. 193 (2018) 86–90, https://doi.org/10.1016/j.mee.2018.02.027.
[36] M. Mattmann, C. Roman, T. Helbling, D. Bechstein, L. Durrer, R. Pohle, M. Fleischer, C. Hierold, Pulsed gate sweep strategies for hysteresis reduction in carbon nanotube transistors for low concentration NO2 gas detection, Nanotechnology 21 (18) (2010), https://doi.org/10.1088/0957-4484/21/18/185501.
[37] M. Muoth, T. Helbling, L. Durrer, S.-W. Lee, C. Roman, C. Hierold, Hysteresis-free operation of suspended carbon nanotube transistors, Nature Nanotechnol. 5 (8) (2010) 589–592, https://doi.org/10.1038/nnano.2010.129.
[38] S. Heinze, J. Tersoff, R. Martel, V. Derycke, J. Appenzeller, P. Avouris, Carbon nanotubes as schottky barrier transistors, Phys. Rev. Lett. 89 (10) (2002) 106801, https://doi.org/10.1103/PhysRevLett.89.106801.
[39] A. Ortiz-Conde, F.J. García Sánchez, J.J. Liou, A. Cerdeira, M. Estrada, Y. Yue, A review of recent MOSFET threshold voltage extraction methods, Microelectronics Reliability 42 (4-5) (2002) 583–596, https://doi.org/10.1016/S0026-2714(02)00027-6.
[40] S. Rumyantsev, G. Liu, M.S. Shur, R.A. Potyrailo, A.A. Balandin, Selective gas sensing with a single pristine graphene transistor, Nano Lett. 12 (5) (2012) 2294–2298, https://doi.org/10.1021/nl3001293.
[41] E. Commission, Air Quality Standards, (2016).
[42] R.J. Chen, N.R. Franklin, J. Kong, J. Cao, T.W. Tombler, Y. Zhang, H. Dai, Molecular photodesorption from single-walled carbon nanotubes, Appl. Phys. Lett. 79 (14) (2001) 2258–2260, https://doi.org/10.1063/1.1408274.
[43] J.P. Shi, R.M. Harrison, Regression modelling of hourly NO(x) and NO2 concentrations in urban air in London, Atmospheric Environ. 31 (24) (1997) 4081–4094, https://doi.org/10.1016/S1352-2310(97)00282-3.
[44] P. Anttila, J.P. Tuovinen, J.V. Niemi, Primary NO2 emissions and their role in the development of NO2 concentrations in a traffic environment, Atmospheric Environ. 45 (4) (2011) 986–992, https://doi.org/10.1016/j.atmosenv.2010.10.050.
[45] R. Kurtenbach, J. Kleffmann, A. Niedojadlo, P. Wiesen, Primary NO2 emissions and their impact on air quality in traffic environments in Germany, Environ. Sci. Europe 24 (6) (2012) 1–8, https://doi.org/10.1186/2190-4715-24-21.
[46] D. Zhang, P. Solomon, S.L. Zhang, Z. Zhang, Correlation of low-frequency noise to the dynamic properties of the sensing surface in electrolytes, ACS Sens. 2 (8) (2017) 1160–1166, https://doi.org/10.1021/acssensors.7b00285.
[47] I. Heller, J. Mannik, S.G. Lemay, C. Dekker, Optimizing the signal-to-noise ratio for biosensing with carbon nanotube transistors, Nano Lett. 9 (1) (2009) 377–382, https://doi.org/10.1021/nl8031636.
[48] N.K. Rajan, X. Duan, M.A. Reed, Performance limitations for nanowire/nanoribbon biosensors, Wiley Interdisciplinary Reviews: Nanomed. Nanobiotechnol. 5 (6) (2013) 629–645, https://doi.org/10.1002/wnan.1235.